Available online at www.sciencedirect.com
ScienceDirect
Journal of Power Sources 179 (2008) 520–531
JOURNAL OF POWER SOURCES
www.elsevier.com/locate/jpowsour

Novel proton-exchange membrane based on single-step preparation of functionalized ceramic powder containing surface-anchored sulfonic acid

S. Reichman [a], L. Burstein [b], E. Peled [a,*]

[a] *School of Chemistry, Tel-Aviv University, Ramat Aviv, Tel Aviv 69978, Israel*
[b] *Wolfson Applied Materials Research Center, Tel-Aviv University, Ramat Aviv, Tel Aviv 69978, Israel*

Received 4 September 2007; received in revised form 24 October 2007; accepted 16 December 2007
Available online 20 January 2008

Abstract

A novel approach to the synthesis of a low-cost proton-exchange membrane (PEM) based on the single-step preparation of a functionalized ceramic powder containing surface-anchored sulfonic acid (SASA) and a polymer binder, is presented for the first time. The added value of this technique, compared with earlier work published by our group, is the adoption of a direct, single-step synthesis, as opposed to a multiple-step synthesis. The latter requires an oxidation step, in order to convert the thiol group into a sulfonic group. SASA powders of different compositions have been prepared and characterized by means of Brunaur–Emmet–Teller (BET), thermogravimetric analysis–differential thermal analysis (TGA–DTG), differential scanning calorimeter (DSC), Fourier transformation infrared (FT-IR), nuclear magnetic resonance (NMR), X-ray photoelectron spectroscopy (XPS), atomic force microscopy (AFM), scanning electron microscopy (SEM) and electrochemical techniques. The lowest equivalent weight measured for SASA powders is 1281 g equiv.$^{-1}$. The ionic conductivity of a 100-μm-thick membrane is measured *ex situ* at room temperature (25 ± 3 °C) and the highest proton conductivity is 48 mS cm^{-1}. The typical pore size, for the SASA powders is less than 10 nm and ranges from 2 to 50 nm for the SASA-based membranes. The membranes are thermally stable up to 250 °C.

Direct methanol fuel cells (DMFCs) are assembled with some of the membranes. Preliminary tests showed that the cell resistance for a ∼100-μm-thick membrane ranges between 0.29 and 0.19 Ω cm^2 from 80 to 130 °C, respectively, and that the maximum cell power density with a 1 M methanol solution is 127, 208 and 290 mW cm^{-2} at 80, 110 and 130 °C, respectively, while the corresponding methanol crossover current density is 0.093, 0.238 and 0.281 A cm^{-2}.

Keywords: Composite proton-exchange membrane; Membrane electrode assembly; Surface-anchored sulfonic acid; Direct methanol fuel cell; Functionalized ceramic powder; Power density

1. Introduction

For the last decade, proton-exchange membrane fuel cells (PEMFCs) have been explored as the technology of choice for clean and efficient energy-conversion systems for automobiles, portable applications, and stationary power generation. The proton-exchange membrane (PEM) is a central and critical component in PEMFCs. The membrane must possess a suitable combination of the following properties—high proton conductivity, good mechanical and chemical properties, low permeability to gases, limited swelling in the presence of water, and fabrication costs appropriate for the application [1–3]. As a result, there is much interest in the study and development of such membranes.

One of the major problems with perfluorosulfonic-acid (PFSA) membranes has been, and still is, their high cost (∼US$ 700 m^{-2}). This is due to the expensive fluorination step and lengthy preparation required for manufacture, thus creating an incentive for creating other types of membrane [4]. Nafion® (E.I. du Pont de Nemours & Co. Inc.), the ubiquitous membrane and the technology standard, is by far the most studied proton-conducting electrolyte and operates in fuel cells at near-ambient temperature (up to 80 °C). In direct methanol fuel cell

* Corresponding author at: Sackler Faculty of Exact Sciences, Tel-Aviv University, Ramat Aviv, Tel Aviv 69978, Israel. Tel.: +972 3 640 8438; fax: +972 3 641 4126/640 9293.
E-mail addresses: reichman@tau.ac.il (S. Reichman), burstein@eng.tau.ac.il (L. Burstein), peled@tau.ac.il, peled@post.tau.ac.il (E. Peled).

0378-7753/$ – see front matter © 2008 Elsevier B.V. All rights reserved.
doi:10.1016/j.jpowsour.2007.12.127

(DMFC) applications, Nafion® membranes present, in addition to their high cost, four major disadvantages, namely: (i) marked dependence of the conductivity on its water content (high osmotic drag, which makes water management at high current densities difficult); (ii) sensitivity to metal-ion impurities; (iii) poor thermal stability at above 100 °C; (iv) very high methanol crossover [5]. For Nafion® 117, the crossover current density is 125–150 and 250–300 mA cm^{-2} for 1 M methanol at 60 and 90 °C, respectively [6–8]. Methanol, crossing over from the anode side through the Nafion® membrane to the cathode side, reacts with oxygen, produces heat, and reduces the energy-conversion efficiency.

In recent years, there has been an intensive effort to develop a low-cost membrane to replace Nafion®, and significant progress has been made [9–19]. Various membranes, such as sulfonated aromatic-polymer films [13–15], radiation-grafted membranes [16], sulfonated polysulfones, perfluorinated sulfonamides [17], sulfonated polyetherketones and sulfonated polyetheretherketones [18], with basic polymers such as poly(4-vinylpyridine), polybenzimidazole, or substituted polysulfones have been synthesized in attempts to develop a suitable DMFC membrane [19]. The sulfonation of these polymers leads however, to the formation of water-soluble polymers at high sulfonation levels.

We have reported on the development of a novel nanoporous proton-conducting membrane (NP-PCM), which consists of ceramic powder, polymer binder (PVDF) and aqueous acid, and on a DMFC and a direct ethylene glycol fuel-cell based on this membrane [12,20–22]. The NP-PCM has several advantages over the commercial Nafion® membrane, viz., more than two-orders-of-magnitude lower membrane cost, relative insensitivity to metal-ion impurities, higher water permeation under hydraulic pressure, and up to an order-of-magnitude lower fuel crossover. The rapid water permeation also enables the use of a liquid–water barrier layer for internal water recycling, thus avoiding the necessity of a water-recycling pump [23,24]. It also reduces the relative humidity of the air (oxygen) that exits the cathode.

As none of the previously reported membranes had a sufficiently long operating life at above 100 °C, it was decided to use the most stable polymer, i.e., PTFE, as the binder in the NP-PCM [25,26]. The membrane consists of a PTFE-based matrix doped (*via* an acid-catalyzed *in situ*, sol–gel technique) with nanosize silica particles that have good acid-adsorption capacity, and an aqueous acid solution that fills the nanosize pores.

Although NP-PCMs allow for variations in the type of aqueous acid that can be used to fill the nanopores, one of the disadvantages in using an aqueous acid (e.g., a perfluorosulfonic acid, like trifluoromethanesulfonic acid) is the need to incorporate corrosive-resistant hardware components into the fuel-cell system. Therefore, with the aim of developing a low-cost, high-temperature membrane, we have synthesized and characterized novel composite proton-exchange membranes (CPEMs), based on a single-step preparation of a functionalized ceramic powder containing surface-anchored sulfonic acid (SASA). Preliminary results, which incorporate similar SASA techniques, have been recently published [27]. The added value in this technique, compared with earlier work, published by our group, is the adoption of a direct single-step synthesis as opposed to a multiple-step synthesis; the latter requires an oxidation step, in order to convert the thiol group into a sulfonic group to obtain an improved CPEM.

The above membranes consist of a polymer binder (PVDF) and a nanosize ceramic powder, in which sulfonic-acid groups are anchored to the surface of the powder *via* a silane or a perfluoroalkyl-chain linkage. This is unlike Nafion®, in which the sulfonic groups are attached to the polymer backbone. The nanosize ceramic powder particles function as water retainers in the membrane that is an advantage when operating at elevated temperatures.

2. Experimental

2.1. Preparation of SASA powders

Anchoring functional organoceramic powders by means of surface hydroxyl groups has been widely discussed in the literature [28–33]. SASA formation is characterized by two domains: (i) a terminal functional group, which ultimately defines the exposed surface functionality (sulfonic group); (ii) an anchoring group responsible for the specific chemical interactions with the ceramic powder substrate. The convenience of attachment to a wide range of hydroxyl- and/or oxide-bearing surfaces makes silica particularly attractive for surface modification. We have explored the feasibility of several attractive systems that are based on molecules where the anchoring group is a silicon atom with electronegative ligands, typically halides and/or alkoxides. Out of this group, alkoxysilanes, halosilanes and sultones have been examined.

All SASA powders were prepared in a glove box, under an argon atmosphere, with the use of three different precursors and three independent routes (A–C) (Scheme 1). Silica was functionalized with the following precursors: (i) 2-(4-chlorosulfonylphenyl)ethyltrimethoxysilane, 50% solution in methylene chloride ($C_{11}H_{14}ClO_5SSi$, Acros Organics); (ii) 1,2,2-trifluoro-2-hydroxy-1-trifluoromethylethane sulfonic acid beta-sultone ($C_3F_6O_3S$, Matrix Scientific & SynQuest Laboratories, Inc., 98%); (iii) 2-(4-chlorosulfonylphenyl) ethyltrichlorosilane, 50% solution in toluene/methylene chloride ($C_8H_8Cl_4O_2SSi$, Gelest Inc.). 2.0 g of calcined silica (Aerosil® 380, Degussa) was evacuated at 350 °C in a convection oven for 4 h and allowed to cool to room temperature. In route A, a solution of (i) above (4 mL) in 90 mL anhydrous methylene chloride (CH_2Cl_2, Gadot Laboratories, AR) and 0.5 mL glacial acetic acid (CH_3COOH, Frutarom, ≥99%) was added and the mixture was inserted by syringe in a septum-capped round-bottom one-neck flask, to give a final silane concentration of ∼2% (v/v). The mixture was left to reflux overnight, under an inert atmosphere of nitrogen, at room temperature. In route B, a solution of (ii) above (0.4–1.2 mL) in 50–70 mL anhydrous toluene ($C_6H_5CH_3$, Aldrich, 99.8%) was added and the mixture was inserted by syringe in a septum-capped round-bottom three-neck flask, to give a final sultone concentration of ∼8–26% (v/v), respectively. The mixture was refluxed for 6 h under an inert atmosphere of nitrogen at 110 °C. In route C, a solution

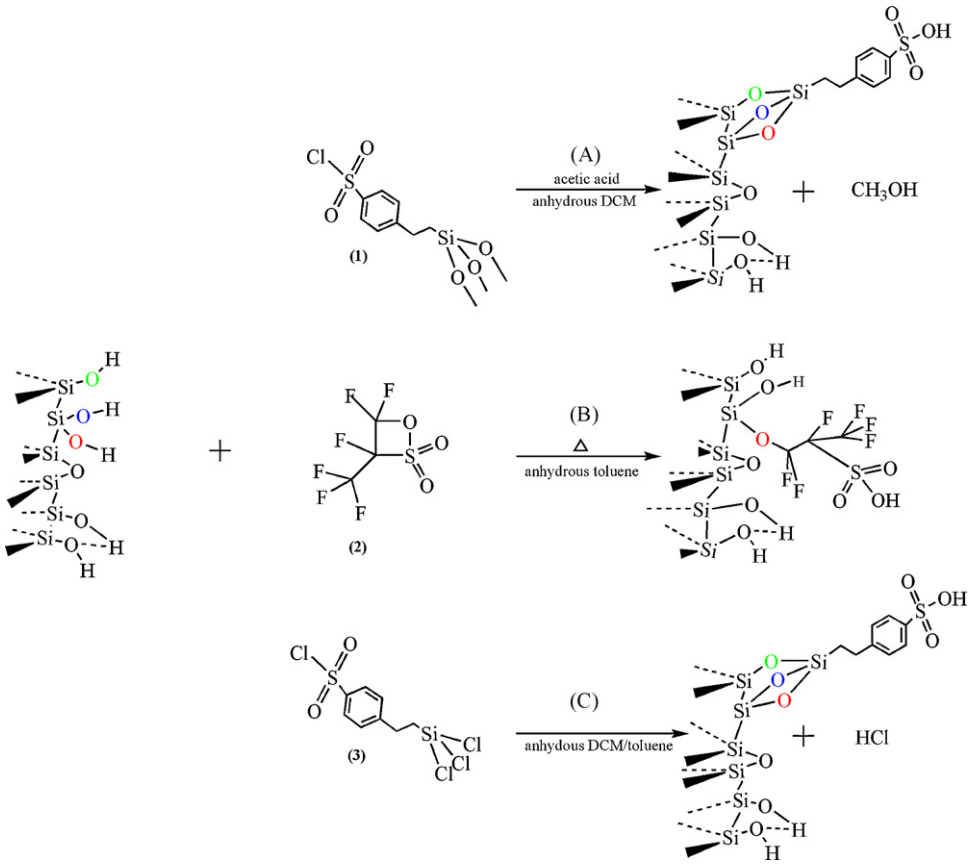

Scheme 1. Representation of surface-anchored sulfonic acid (SASA) groups attached to silica surface *via* free, geminal, vicinal and bridged silanol groups, by use of three different precursors (i)–(iii) and three independent routes A–C.

of (iii) above (4 mL) in 90 mL anhydrous toluene/methylene chloride was added and the mixture was inserted by syringe in a septum-capped round-bottom one-neck flask, to give a final silane concentration of ∼2% (v/v). The mixture was left to reflux overnight, under an inert atmosphere of nitrogen, at room temperature.

In all three routes, filtration of the solids was carried out by first washing the solids thoroughly with the relevant solvent: methylene chloride in (i), toluene in (ii), and toluene/methylene chloride in (iii)—in order to remove any unreacted precursor or by-products. These washings took place at room temperature and were conducted four times. Following this, five more washings were carried out with de-ionized water at 50 °C until a neutral pH of the solids was achieved. Each washing was done with 50 mL of either solvent or water and the sample was centrifuged (IEC) at 2500 rpm for 5 min. The solids were left to dry overnight at 100 °C in a vacuum oven. Finally, the solids were ground into fine powder by mixing with *iso*-propyl alcohol (C_3H_8O, Frutarom Ltd., CP) solution in a mortar and pestle and allowing the solvent to evaporate.

2.2. Fabrication of SASA membranes

SASA membranes were prepared by a solvent-casting technique [12] with the use of a K control coater (RK Print, Coat Instruments) on a glass substrate. The viscous paste was formed by mixing nanosize ceramic SASA powders with poly(vinylidene difluoride) (PVDF, Kynar 2801-00 ELF Autochem). The final porosity of the membrane was calculated to be 60%, the remaining 40% consisting of solids: 12% (v/v) nanosize ceramic SASA powder and 28% (v/v) PVDF polymer. The paste was poured into the coater to form a wet film. Upon evaporation of the solvent, a flexible film was obtained.

The membrane was washed several times with organic solvents and with de-ionized water. Using this procedure, three CPEMs, were prepared and consisted of PVDF and SASA powders, synthesized by the three routes described above.

2.3. MEA preparations

The membrane electrode assembly (MEA) was prepared by hot-pressing the electrodes on to the CPEM at 100 °C and 25 kg cm^{-2} for 30 s. The electrode area of a single cell was 5 cm^2. The anode catalyst was a platinum–ruthenium (50:50 at. wt.%) nanopowder (platinum–ruthenium black, Alfa Aesar, HiSPEC^{TM} 6000). It was spread three times over un-teflonated carbon–fiber paper (Toray, Inc., Japan) by a paint-brush technique, in both vertical and horizontal directions, with drying at room temperature between applications. The cathode was a commercial E-TEK® electrode (De Nora Elettrodi). It was hand-fabricated by coating it on one side, with unsupported, high-power Pt-black, and 0.6 mg cm^{-2} Nafion®. The platinum loading of both the anode and the cathode was 4 mg Pt cm^{-2}.

2.4. Fuel-cell testing

The fuel-cell housing was built from blocks of synthetic graphite (Poco Inc.), in which flow-fields were engraved [26]. Preliminary performance tests of a non-optimized DMFC were carried out. An aqueous solution of 1 M methanol (CH_3OH, Frutarom, analytical grade) was circulated through the anode compartment at a flow rate of 40 mL min^{-1}. Dry air was fed, at 0.05–3 bar (abs), into the cathode compartment at a rate of 90–240 mL min^{-1}.

The cell resistance was measured *in situ* by a.c. perturbation from 1 MHz to 1 kHz with the use of a Solartron model SF 1260 AC analyzer.

The crossover current density was measured [20,34] by applying a positive voltage at the cathode (while flushing it with nitrogen) in order to oxidize the methanol that crossed over.

2.5. Characterization methods

The SASA powders were back-titrated in order to determine their equivalent weight (EW). SASA powder samples of measured weight (*ca.* $0.15 \pm 1 \times 10^{-5}$ g) were immersed in de-ionized water at 70 °C and rinsed repeatedly until a constant pH was achieved. Samples were vacuum-dried at 60 °C for 12 h and then immersed in 20 ± 0.06 mL of 0.01 M sodium hydroxide (NaOH, Merck, GR) for 24 h in sealed Erlenmeyer flasks. The sodium hydroxide solution was titrated with 0.01 M hydrochloric acid (HCl, BioLab Ltd., 32% (w/w) CP) until a bromocresol-green ($C_{21}H_{14}Br_4O_5S$, Merck, ACS reagent) endpoint was reached. Under the assumption of complete conversion of the sulfonic-acid proton of the SASA powder samples, the EW was calculated *via* the following equation:

$$\mathrm{EW} = \frac{m_{\mathrm{SASA\ powder}}}{n_{\mathrm{NaOH}} - n_{\mathrm{HCl}}} \quad (1)$$

where $m_{\mathrm{SASA\ powder}}$ is the weight of the SASA powder sample, n_{NaOH} is the number of moles of sodium hydroxide initially added and n_{HCl} is the number of moles of sodium hydroxide back-titrated with hydrochloric acid.

For each of the EW measurements presented for each powder, at least three samples were taken. The EW of a Nafion®117 membrane was titrated in the same way and used as reference.

The pore-size distribution (PSD) of dry silica powders, SASA powders and SASA-based membranes was measured with a NOVA 2200 Quantachrome Autosorb Automated Surface Area gas-sorption analyzer based on the density-functional theory (DFT). Samples were dried and degassed prior to their examination.

The TGA tests were carried out with a TA Instruments model SDT 2960 instrument. The runs were recorded at a scan rate of 10 °C min^{-1} up to 700 °C. The sample compartment was flushed with dried argon (UHP) at all times. The DSC tests were carried out with a TA Instruments module 2010 and System Controller 2100. DSC runs were recorded at a scan rate of 10 °C min^{-1} over the temperature range of 25–300 °C. Membrane samples were sealed in alodined (covered by high-resistant and compact surface-oxide film) aluminum DCS pans.

Spectroscopic characterization of the SASA powder samples was obtained by means of a Smiths Detection (model TravelIR II IdentifyIR) diamond-attenuated-total-reflection (D-ATR) Fourier transformation infrared (FT-IR) spectrometer in the 700–4000 cm^{-1} range. Also measured was ^{1}H NMR, recorded on a Bruker Avance-200 MHz NMR spectrometer. The ^{1}H spectrum was referenced to the ^{1}H water peak in deuterium oxide (4.83 ppm) and 100 scans were recorded. Samples were prepared by inserting 17 mg of dry SASA powder into 5 mm NMR sample tubes, which were suspended in 0.5 mL deuterium oxide.

In order to evaluate the chemical composition of the various SASA powders, X-ray photoelectron spectroscopy (XPS) measurements were performed with the use of a 5600 Multi-Technique System (PHI, USA). The samples were irradiated with an Al Kα monochromated source (1486.6 eV). The samples were analyzed at their surface only. Sample charging was compensated with a charge neutralizer. The carbon peak at 284.05 eV was used as an energy reference for all the measured peaks. High-resolution spectra were taken at a pass energy of 11.75 eV, at an increment of 0.05 eV $step^{-1}$.

The morphology of the surface area and cross-section of the membrane were determined by scanning electron microscopy (SEM) analysis (JSM-3600, JEOL). A low-voltage value of 5 kV was used to avoid electron-beam damage to the membrane samples. A sputtered gold coating with a thickness of 200 Å was achieved with the use of a Polaron SC 500 Sputter Coater (Fisons Instruments). Cross-sections of both membrane and MEA samples were prepared by dipping them in liquid nitrogen in order to break them. Atomic force microscopy (AFM) was employed for imaging the surface of SASA-based CPEMs with an AutoProbe CP Research AFM System (ThermoMicroscopes). A silicon–nitride cantilever with a curvature radius of 40 nm was used for contact mode in air and at room temperature. Membrane samples were dried at 60 °C for several hours, before being examined.

The ionic conductivity of the SASA-based PCM, held between two gold-plated electrodes (1 cm^2), was measured at room temperature (25 ± 3 °C) with a Solartron model SF 1260 AC analyzer. The electrodes were pressed between two stainless-steel plates and clamped tightly by two bolts. Between the electrodes and the membrane, a gas-diffusion layer (De Nora Elettrodi, hand-fabricated single-sided coating, unsupported, 30% (w/w) PTFE) was placed on each side of the membrane to improve the electrical contacts with the interphase. Before these measurements were made, samples of the membrane were immersed in a 3 M aqueous solution of sulfuric acid (H_2SO_4, Merck, 95–97%, GR for analysis) for 1 h at 70 °C. The residual acid was then removed by immersing the samples in de-ionized water at 80 °C for 4 h, until neutral pH was obtained. For each ionic-conductivity measurement, at least three samples of the membrane were examined.

The water-permeation rate under static hydraulic water pressure for the SASA-based membranes was measured and compared with that of other NP-PCMs of our group and a Nafion® 117. This was made possible by clamping the membrane sample (*ca.* 100 μm thick) in a ball joint sealed with an

O-ring, attached to a glass tube. The upper end of the tube was covered with a paraffin film to prevent loss of water by evaporation. The tube was filled with water to an initial height of 500 mm. The hydraulic water permeation φ was calculated by measuring the drop in the water level h, using the following equation:

$$\varphi = \frac{h \times \rho}{t} \times 1000 \quad (2)$$

where ρ is the density of water at room temperature and t is the total number of hours during which hydraulic water permeation took place. The water-permeation rate was calculated in units of mg h^{-1} cm^{-2}. All membrane samples consisted of 12% (v/v) ceramic powder.

Contact-angle measurements were carried out at room temperature by placing a droplet of water, with a syringe (B&D Microlance 3) directly on a dry, flat SASA-based CPEM sample. The perceived contact angle of the droplet with the membrane surface was measured with a goniometer on a photographed image. An average contact angle was determined from 10 measurements with an experimental error of 2–3°.

To conduct the bubble-point test, the membrane was incorporated in the fuel-cell hardware as part of the MEA. The bubble point was measured in that manner in order to test the permeability of the membrane to gas under *in situ* conditions. Nitrogen was then passed through the cell from one side and water through the opposite side (at room temperature). The nitrogen pressure was increased, until bubbles were observed in the water stream.

3. Results and discussion

The SASA powders are composed of high-surface area, electronically non-conductive particles with good retention capability for water. Covalent anchoring of the sulfonic acid functional groups to the silica surface are achievable by a direct, one-step synthesis *via* an S_N2 mechanism reaction. The hydroxyl groups from the silanol on the silica surface act as nucleophiles, in which the oxygen atom on the hydroxyl bond has a lone pair that is available to be used in order to form a 'new' sigma bond to the electrophilic silicon on the precursor. As a result, either chloride or methoxide act as leaving groups in the reaction, depending on the precursor chosen. Because methoxide is considered to be a poorer leaving group, as in the use of route A with precursor (i), compared to halides (*i.e.* chlorides in route C), an acidic catalyst (glacial acetic acid) is incorporated in the reaction, thereby enabling the formation of methanol, which is a stronger leaving group. On the other hand, the cyclic precursor (ii) in route B reacts with the surface silanol groups of the silica by opening the sultone ring and forming a covalent bond between the silica framework and the perfluoroalkyl chain with terminal sulfonic acid functional groups [35].

The advantage of these three synthesis routes lies in the fact that the anchoring and formation of the sulfonic group is achieved in a single step, in contrast with previous work found in the literature, in which a rather inefficient thiol oxidation is needed after the anchoring [36,37].

Table 1
EWs, measured by back-titrations, of the various SASA powders synthesized *via* routes A–C

Sample measured	EW (g equiv.$^{-1}$)
Nafion® TM 117	1221
SASA product (A)	1313
SASA product (B)	2510
SASA product (C)–DCM	1676
SASA product (C)–toluene	1281

The ionic conductivity of the membranes is important in achieving high power densities for the fuel cell. Membrane conductivity is strongly influenced by the water content [38]. A number of factors affect the water content, including the cation form and the ion-exchange capacity of the membrane. Since the membrane is based on SASA powder, its EW depends on that of the powder (grams of powder per mole of fixed sulfonate sites). A decrease in EW would lead to an increase in conductivity. The calculated value for the EW of a pure, silica-based ceramic powder is based on the manufacturer's value of silanol-group density, silanol-group concentration and the relevant specific surface area (BET) [39]. On the assumption of complete conversion during the reaction, so that the number of acid groups is equivalent to that of the silanol groups, the EW of the SASA powder was calculated to be about 600–1600 g equiv.$^{-1}$ for surface areas of 380–150 m^2 g^{-1}, respectively. Obviously, we were most interested in obtaining a low EW and thus chose a silica-based ceramic powder which, to date, attains the highest specific surface area for silica, the highest value of silanol-group density, and the highest value of silanol-group concentration.

The calculated EWs presented here are in the useful range of EWs (600–1600 g equiv.$^{-1}$) [9,40], between the solubility and percolation limits and thus show great promise. Back-titrations of the SASA powders were performed and the EWs of these powders were calculated. The SASA-based CPEM consists of 31% (w/w) SASA powder and 25% (w/w) PVDF. Some of the EWs of the various SASA powders are somewhat higher than the minimal calculated values of 600–1600 g equiv.$^{-1}$ (Table 1). The EW calculated for the reference Nafion® 117 membrane was slightly higher than the manufacturer's indicated value (1100 g equiv.$^{-1}$). This indicates that the actual EW values of our SASA-based membranes are, to some extent, lower than those measured here. As it is quite difficult to titrate a 'solid' acid, the values measured as the EWs are thus regarded as upper limiting values. The results may also indicate that either the sulfonation or silanization process, or both, were not complete and that not every silanol group is associated with an acid group.

In order to allow sequential contact between the adjacent sulfonic acid groups, an important structural requirement must be fulfilled, namely, the polymer binder which supports the SASA powder must not cover it completely (Scheme 2). The gap between two adjacent SASA particles must be as small as possible in order to allow continuous and rapid transport of protons. Although a variety of SASA powders and membranes was prepared *via* different precursors, in this paper we present results on a narrow range of SASA powders and membranes that incor-

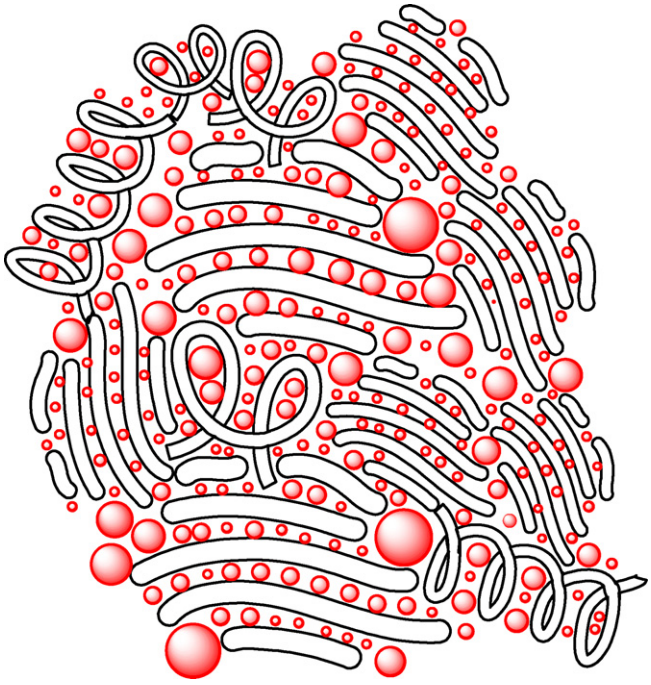

Scheme 2. Idealized representation of a model depicting the SASA powder, supported by a polymer binder, but not entirely covered by it.

porated route C and the toluene-based precursor (iii). The route stated above, as seen when measuring the EW of the SASA powder, exhibits the greatest potential in achieving the final goal of developing a conductive membrane and therefore its properties and performance were further examined. If the fact that the membrane also contains PVDF is taken into account, the effective EW of the membrane should be somewhat higher (2314 g equiv.$^{-1}$) than the initial SASA powder (1281 g equiv.$^{-1}$). Better results are observed when toluene is used as a solvent in route C instead of methylene chloride, since toluene is a more bulky solvent, compared with methylene chloride. Thus, toluene is less likely to intercalate between the surface groups *via* van der Waals bonds and leave voids.

The PSD measurements of a typical dry sample of SASA powder, calculated by the DFT method, reveal two abundant groups of pores, smaller than 10 nm (Fig. 1). The first and more prominent pore volume of the two groups of pores is at a pore width of less than 3 nm, it reaches a maximum value at ~2 nm. The pore width of the second group ranges from 6 nm and decreases progressively up to ~20 nm. When compared with a dry silica powder, the same maximum pore volume is at ~2 nm with a longer tail. The value obtained for the PSD of the dry silica powder is of the same order as that of the characteristic physicochemical data (7 nm average primary-particle size) published by the manufacturer [39]. By means of PSD measurements, it is found that the functionalization process renders a PSD larger than that of the dry silica powder. Since the pore width of the second group of pores in the SASA powder is much more distinct than that of the dry silica powder, it is concluded that agglomeration takes place during the functionalization reaction of the dry silica powder. The addition of functional groups to the silica causes a decrease in the volume of the smallest, 2 nm, pores and

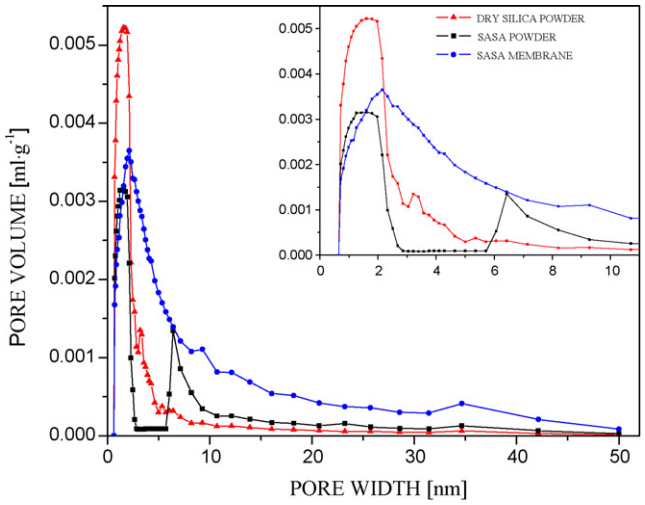

Fig. 1. Pore-size distribution (PSD) of dry silica powder (average primary particle size 7 nm), typical SASA powder (~2% (v/v) silane) and SASA-based membrane.

the formation of another group of pores at about 7 nm. The PSD of the SASA-based membranes reveals a wider spectrum of pore sizes, ranging from 2 to 50 nm, when compared with the SASA and dry silica powders. Nevertheless, the volume peak is still at 2 nm. In the fuel cell, all these pores are filled with water and thus permit ionic conduction. They are small enough to maintain a large gas-pressure gradient when filled with water, as seen from bubble-point measurements. For comparison, Nafion® has a wide spectrum of pore sizes ranging from 1 to 100 nm, with an average value of about 2 nm [41].

The results of the thermal analysis of the SASA powders and membranes are shown in Figs. 2 and 3. All SASA powders are stable up to 350 °C (Fig. 2). There is a 2–7% weight loss at the beginning of the heating run. This is assigned to the release of adsorbed surface water. Comparing the temperature at which this weight loss occurs for the various SASA powders and that of a dry silica powder reveals a difference in temperature range:

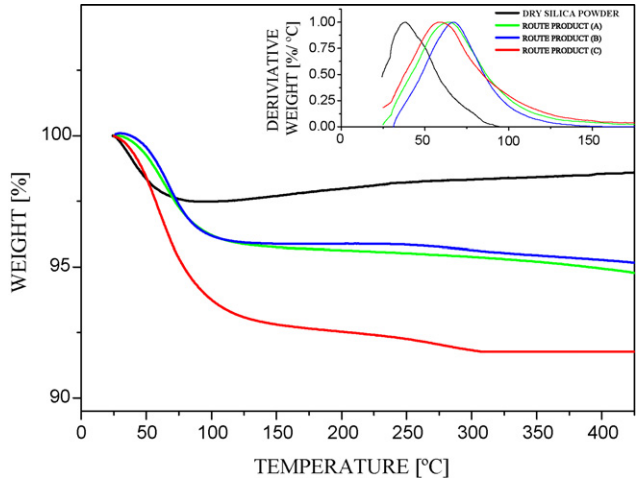

Fig. 2. TGA curves of SASA powders prepared *via* routes A–C and compared with dry silica powder. In the insert, DTG curves of SASA powders prepared *via* routes A–C are compared with that of dry silica powder, indicating a difference in the manner in which water molecules are adsorbed on powder surface.

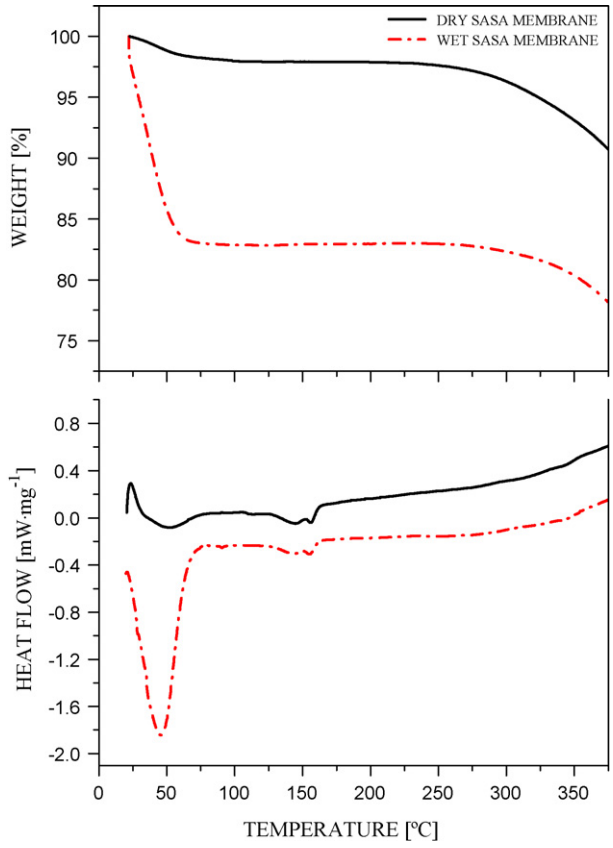

Fig. 3. TGA and DSC tests for dry and wet SASA-based membranes, synthesized by route C and the toluene-based precursor (iii).

a weight loss at 60–65 °C is observed for the three different SASA powders, while it takes place at 37 °C for the dry silica powder. This distinct difference in temperatures indicates a difference in the manner in which water molecules are adsorbed on the surface of the powders, two energetically different surface sites, and thereby demonstrates the different chemistry of surface groups of the SASA powder (insert Fig. 2). The larger water loss of the SASA powders in comparison with that of the silica powder indicates extra water bound to the sulfonic groups. A two-stage phase transition (which is not shown here) is apparent for membranes obtained *via* routes A and C, between 400 and 600 °C. This transition is associated with the decomposition of the organic molecule anchored to the SASA powder. The difference in chemical structure obtained *via* route B, fluorocarbon compared with hydrocarbon in routes A and C, does not exhibit a phase transition at the temperature range specified above. Second runs of the various SASA powders do not indicate decomposition or weight loss and thus indicate an irreversible process.

Fig. 3 shows the results of TGA and DSC tests for dry and wet SASA-based membranes incorporating precursor (iii) in toluene *via* route C. SASA-based membranes are found to be thermally stable up to 250 °C. As in the case of the SASA powders, there is an endothermic 2% weight loss at about 40 °C on heating of the dry membrane and almost 15% weight loss for the wet membrane. It will be noted that the low-temperature weight loss is smaller in the dry membrane than it is in the SASA powders. This

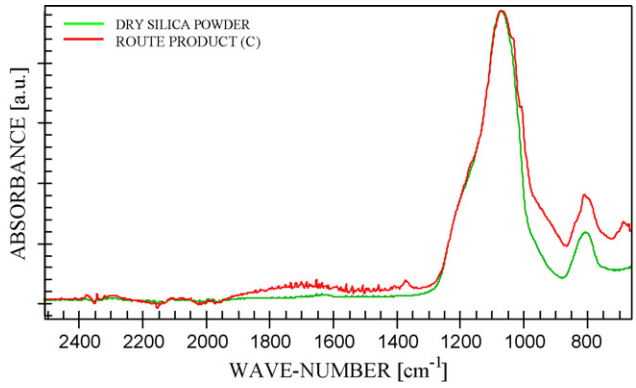

Fig. 4. Representative FT-IR spectroscopy of dry silica powder compared with SASA powder obtained *via* route C and the toluene-based precursor (iii), showing characteristic reflectance bands in wave-number range of 650–2500 cm^{-1}.

can be explained by the lower content of silica in the membrane, due to the presence of the polymer binder, PVDF. In the DSC curves, there is a phase transition appearing in both the dry and wet membranes at 145 °C. This endotherm is most likely associated with melting of the PVDF. A calculation of the enthalpy of fusion of the SASA-based membranes containing 28% (v/v) PVDF, with the use of the enthalpy of fusion of pure crystalline PVDF, reveals that the PVDF of SASA-based membranes has an amorphous character.

FT-IR and ^{1}H NMR spectroscopy were used to ascertain the composition of SASA powder and that of organic residues left during synthesis. The successful introduction of the sulfonate groups was confirmed by FT-IR spectra. A typical IR spectrum of SASA powders obtained by route A or C displays characteristic absorption bands that correspond to sulfonated groups at 900, 1025, 1080, 1370 and 2350 cm^{-1} [35,42,43]. To verify the nature of these absorption bands, the spectrum was compared with dry silica powder (Fig. 4). Since the samples were not fully dehydrated, stretching frequencies are at lower wave numbers than those for the corresponding anhydrous SASA powders. This is due, mainly, to hydrogen bonding between the sulfonic acid groups and water molecules. The stretching-frequency band at 900 cm^{-1} is attributed to the SO bond. The peaks at 1025 and 1080 cm^{-1} assigned to symmetric and asymmetric stretching of sulfonate groups are observed in all the spectra. The band at 1370 cm^{-1} is characteristic of the $\nu_{S=O}$ stretching vibrations of undissociated sulfonic acid groups. The small band at 1680 cm^{-1} is associated with protonated water molecules. The small vibration band at 2350 cm^{-1} is assigned to associated OH groups, due to $-SO_2-OH\cdots H_2O$ hydrogen bonds. C–H stretching vibration bands between 2800 and 3000 cm^{-1} and deformation vibration bands (1400–1500 cm^{-1}) are not detected. This indicates minute, if not undetectable, concentrations of organic residues in the final SASA powder.

The molecular structure of route products A and C was confirmed by ^{1}H NMR (Fig. 5). It shows two aromatic signals at 7.77 and 7.47 ppm, each represented by a doublet ($J = 8$ Hz), indicating the two different hydrogen pairs in the phenyl ring. Two other signals are present at 2.86 and 1.09 ppm. Each of

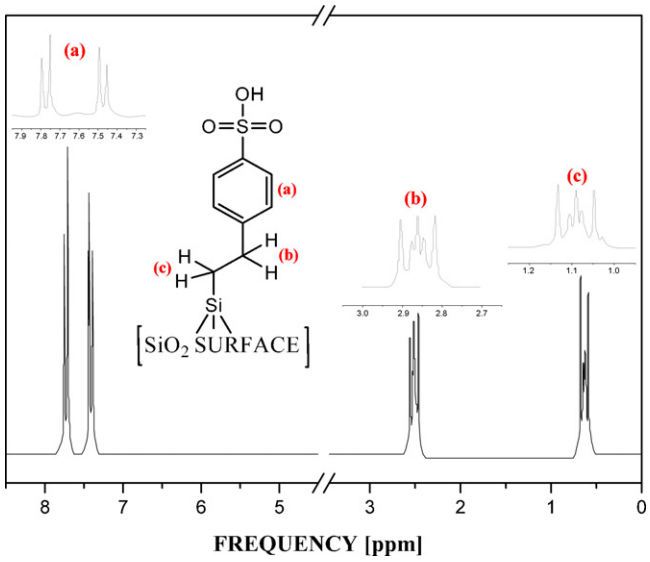

Fig. 5. ^{1}H NMR of molecular structure of products A and C.

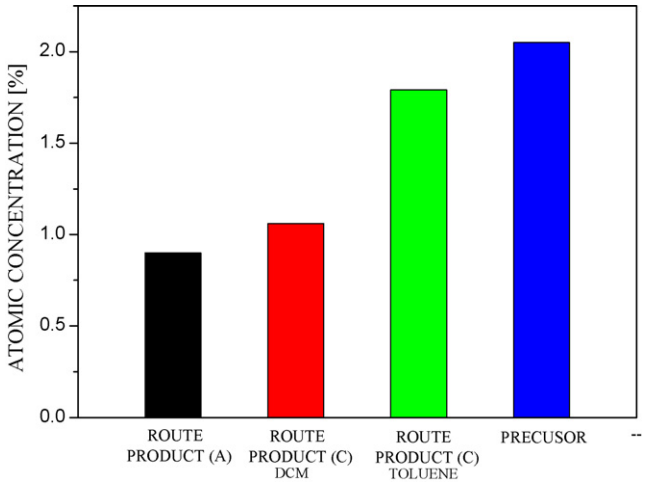

Fig. 6. Atomic concentration of sulfur, at the surface, measured by XPS for route products A and C in both toluene and DCM-based solvents and their relevant precursors.

these two signals are double triplets and are assigned to the aliphatic –CH_2 groups. The first of these two signals is assigned to the group closer to the phenyl ring. The reason for this assignment is due to the electron-withdrawing nature of the aromatic ring, compared with the other aliphatic –CH_2 group, closer to the electron-donating group of the silicon atom. No additional signals are present in the spectra, indicating that no additional residues of the reaction or contaminants are present. The proton of the sulfonic group is not represented in the spectrum as its signal is broad and it undergoes exchange with the water molecules.

XPS analysis was performed in order to characterize the SASA powder, as compared with its precursor involved in route C. This was achieved by measuring the atomic concentration of the elements at the surface of each of the samples. The percentage of the precursor used for each of the samples examined is calculated to be 2% (v/v). If it is assumed that the origin of sulfur is the precursor alone, the yield of sulfur indicates the degree of completion for each of the reactions (Fig. 6). It can be seen that the highest sulfur concentration among the precursors (1.79%) is achieved when precursor (iii) in toluene is incorporated in route C. It can be concluded that this route results in the highest yield of sulfonic acid, assuming that all the sulfur atoms take part in the formation of the sulfonic acid group anchored to the ceramic powder. This is in agreement with its lowest EW.

The XPS spectra of C1s, Si2p and S2s of the measured samples are compared in Fig. 7. The C1s structure of both the SASA powder and precursor (iii) in toluene *via* route C has a maximum at 284.05 eV. The spectrum has an additional peak at about 290.5 eV caused by $\pi \rightarrow \pi^*$ transitions. This peak, typical for aromatic compounds, does not show up in the spectrum of dry silica powder, as expected (not presented here). The shift of the Si2p signal to a higher binding energy for the SASA powder as compared to its precursor can be related to the Si–Cl → Si–O bond exchange process. Oxygen is more electronegative than chlorine (3.4 vs. 3.2, respectively), hence the shift to higher energy suggests that bond exchange does take place. The sulfur S2s structure of both the precursor and the SASA samples is observed at a high binding energy of about 232.5 eV and can be attributed to the sulfonate group bonding [44,45]. A slight shift in the peak maximum, found with the SASA sample, can be attributed to S–Cl → S–O bond exchange in the sulfonic-acid group.

SEM analysis was used to determine the surface and cross-sectional areas of the SASA-based membrane. Fig. 8 shows a cross-sectional area of the membrane and reveals a homogeneous morphology with small recesses and no apparent cracks. The topology of the cross-sectional area of the membrane is similar to that of the surface-area of the membrane.

A three-dimensional-topography AFM image of a SASA-based membrane of 2500 μm^2 area is presented in Fig. 9. The surface plot of the image is not smooth at the nanometer-scale, due to the solvent-casting technique, when casting the membranes on to glass substrates. This is seen in Fig. 9 by the different variations of colour shades – white colour represents membrane areas closer to the cantilever. The height profile of the topography reveals that the depth of the pores fluctuates between 300 and 500 nm. Tiny white spots appear uniformly dispersed throughout the topography of the membrane. They are the pores that fulfill the structural requirement of not being fully covered by the polymer binder, as shown previously in Scheme 2. Submicron roughness helps in achieving good adhesion between the catalyst layer and the membrane.

The ionic conductivity of a 100-μm membrane was measured *ex situ* at room temperature (25 ± 3 °C). The highest proton conductivity is 48 mS cm^{-1}. In another test, the membrane conductivity was calculated from the fuel-cell resistance (measured at high frequency). It increases with temperature from 19 to 46 mS cm^{-1}, at temperatures ranging from 30 to 130 °C, respectively (Fig. 10). This behaviour differs from that of a Nafion® membrane. The latter shows maximum conductivity between 50 and 70 °C and then a decrease above this temperature range [46]. On the other hand, another related study [47] shows that

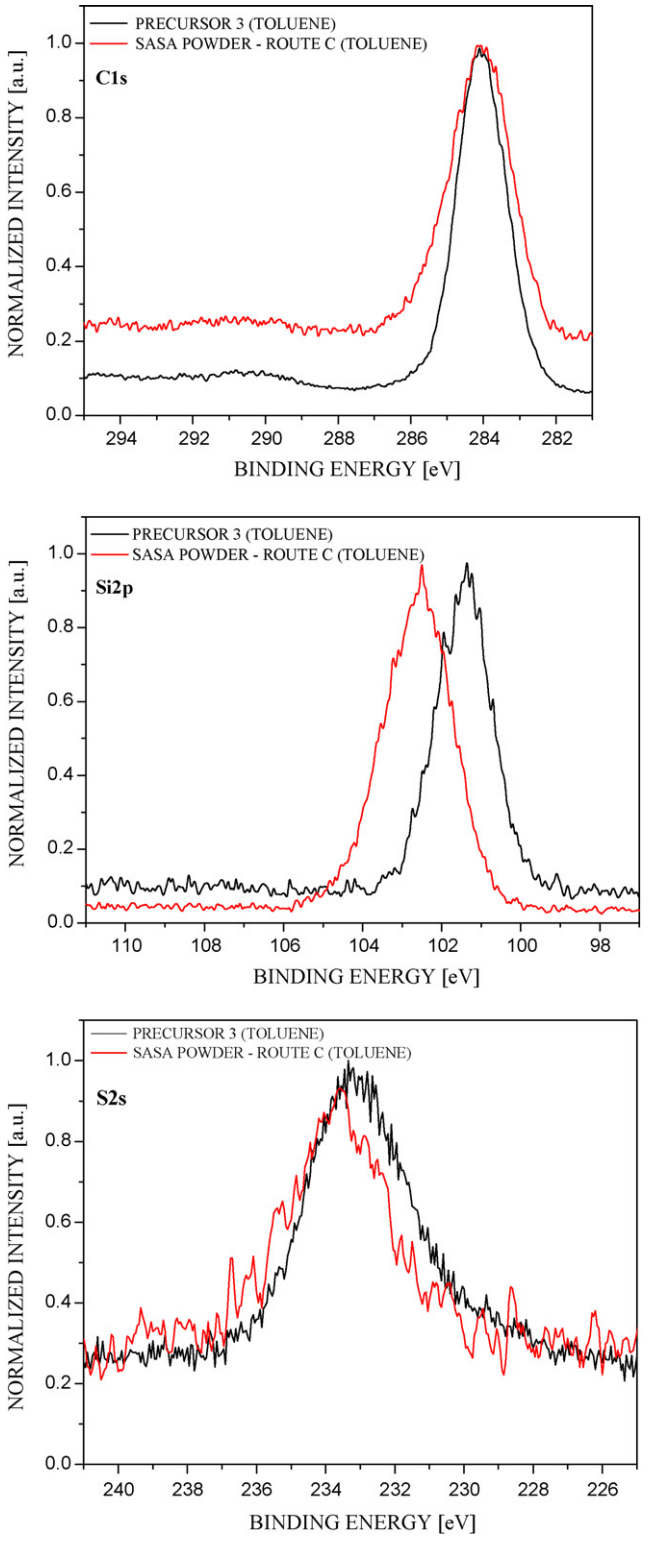

Fig. 7. The XPS spectra of C1s, Si2p and S2s for precursor (iii) in toluene-based solvent and SASA powder *via* route product C.

the conductivity values remain practically constant over a temperature range of 80–160 °C. This suggests that the conductivity growth expected at increasing temperatures is compensated by some modification of the polymer which decreases the mobility and/or the effective concentration of the charge carriers. The

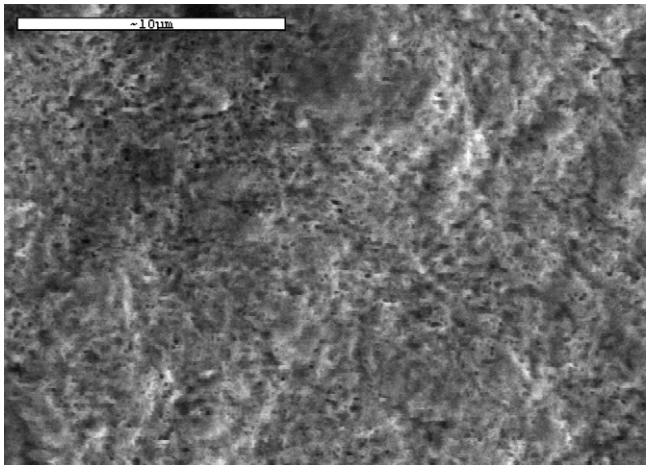

Fig. 8. SEM cross-sectional area micrograph (5000×) of a gold-plated SASA-based membrane pressed at 130 °C for 2 min (100 μm thickness). The membrane sample contains 12% (v/v) ceramic powder.

ionic conductivity exhibits Arrhenius behaviour, showing continuous linearity, an indication that a phase transition does not occur over the temperature range studied. The activation energy is calculated to be 9.5 kJ mol^{-1}. This behaviour differs from that of Nafion®, which does not exhibit continuous linearity. Nafion® has an activation energy of 21 kJ mol^{-1} for conductivity at a constant water content, at low temperatures (30–40 °C). This decreases to 12 kJ mol^{-1} at higher temperatures (up to 70 °C) [48]. Other values of the activation energy for the Nafion® 117 membrane have been published [49–51].

There is not clear correlation between the *ex situ* measured conductivity of the membrane and the *in situ* conductivity measured in the fuel cell. A decrease in ionic conductivity is observed when this is measured under *in situ* conditions in a fuel cell. At

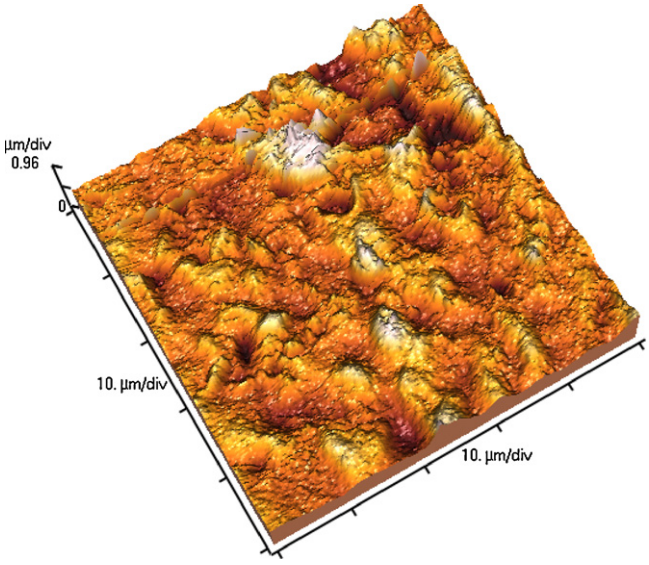

Fig. 9. Three-dimensional AFM topography image of surface of a dry SASA-based membrane, prepared by solution casting on a glass substrate. Imaging is carried out in the contact mode in air and at room-temperature. Image size is 50 μm × 50 μm; light zones correspond to membrane areas protruding above the surface.

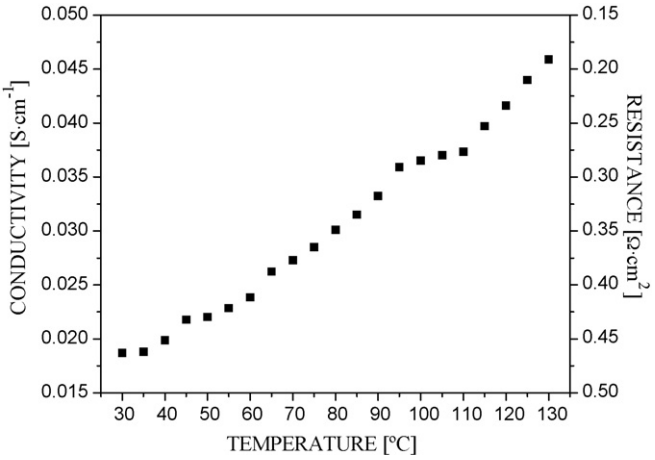

Fig. 10. Membrane conductivity, calculated from the cell resistance. An increase in ionic conductivity (19–46 mS cm^{-1}) is observed as a function of the increase in temperature (30–130 °C), under *in situ* conditions in a DMFC.

room temperature, it is lower by a factor of 2.5. This can be attributed to a possible structure collapse when hot-pressing the membrane for MEA preparation.

The importance of the use of a proton-conducting membrane with high water permeability has been recently demonstrated [24]. It reduces the hydraulic pressure in the cathode-catalyst layer and in the gas-diffusion layer by transferring water through the membrane back to the anode side. This leads to a decrease in cathode flooding and to lower partial pressure of the water vapour in the cathode and in the accompanying flow-field [24]. Both phenomena enable a higher mass transport of oxygen and thus higher power. The water permeation of a membrane depends upon the number, size and shape of the interconnecting hydrophilic pores. The hydraulic water permeation of a SASA-based CPEM was measured and compared with that of previous membranes prepared in our group and referenced to Nafion® 117 [24]. In Fig. 11, it can be seen that the hydraulic water permeation

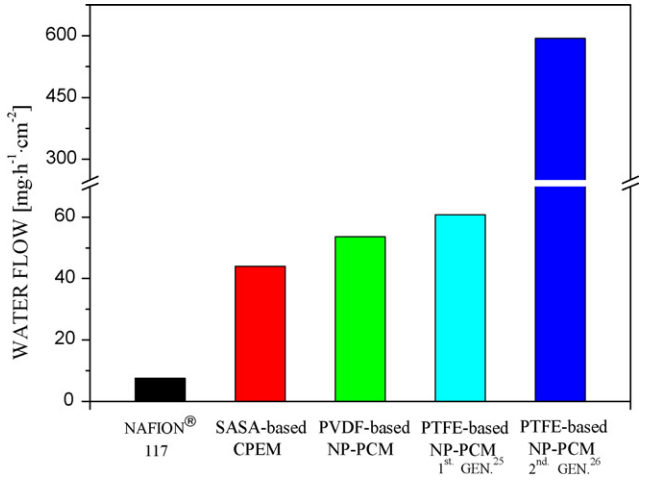

Fig. 11. Hydraulic water permeation of SASA-based membrane compared with that of NP-PCMs of our group and referenced to Nafion® TM 117. Measurements are carried out in a water-column height of 500 mm. All membrane samples are pressed (10,000 psi) and their calculated ceramic powder content is 12% (v/v).

of SASA-based pressed CPEMs is greater than that of Nafion® 117 and relatively similar in magnitude to our previously made membranes.

The measurement of water-contact angles on a SASA-based CPEM reveals a characteristic angle of 75°, which is representative of a hydrophilic, water-attracting material. This value is similar to that we obtained for NP-PCMs, which consist of PVDF and silica only, and is lower than reported in the literature (∼90°), when compared with neat PVDF films [52], and also lower to that measured for Nafion® 115 [53] and 117 [54]. The lower contact angle relative to PVDF and Nafion® could be due to the incorporation of a ceramic powder, which contributes to the wettability of the surface. The functionalized ceramic powder contains sulfonic acid groups that are hydrophilic and thus influence the nature of the PVDF-based substrate. Similar behaviour has been observed with other ceramic powders, when incorporated in a PVDF-based substrate [55].

Bubble-point measurements show that the membrane is able to retain a pressure of at least 4 bar, without bubbles visibly crossing the membrane. This shows that the membrane is appropriate for fuel-cell applications.

Performance tests of several 5-cm^2-area DMFCs with varied membrane thicknesses (∼100 μm) were conducted at 80–130 °C with dry air (Fig. 12a). A methanol solution (1 M) was circulated through the anode compartment at 40 mL min^{-1} and the cathode was fed dry air at 90–240 mL min^{-1} and at 0.05–3.0 bar. The open-circuit voltage (OCV) attained between 80 and 130 °C is in the region of 800 mV. This value is similar to that of a Nafion®-based DMFC. At 80 °C, the cell resistance was 0.29 Ω cm^2 and the maximal cell power density is 127 mW cm^{-2} at 0.05 bar and 1.6 stoich (air) (Fig. 12a). Raising the temperature of the same cell to 110 and 130 °C results in improvement in cell resistance and in the maximum cell power density, namely, 0.23 and 0.19 Ω cm^2, 208 and 290 mW cm^{-2}, at 1.2 and 3.0 bar, 6.3 and 5.5 stoich (air), respectively. The voltage–current curve is linear, typical of a cell with a somewhat high internal resistance. The increase in temperature results in improved performance but also gives rise to a higher crossover rate, compared with fuel-cell performance at 80 °C. The current that flows at 0.9 V is found to be the limiting current for fuel oxidation at all of the temperatures measured. The methanol crossover current density of a 1 M methanol solution obtained at this value of limiting current is 0.093, 0.238 and 0.281 A cm^{-2} at 80, 110 and 130 °C, respectively. This value of crossover is lower than that measured for Nafion® 117 [6–8]. An optimization of the air flow was carried out at 80 °C. The flow of air that was fed to the cathode ranged between 90 and 540 mL min^{-1} at 2.2–14 stoich at 0.35 A cm^{-2}. The maximal cell-power density is found to be 177 mL min^{-1} (4.5 stoich). At lower air flow rates (90–122 mL min^{-1}), the maximum cell-power density decreases by only 5 mW cm^{-2}. This minute drop enables the optimum power density to be achieved for a given temperature while working at practical air flows. At high air flows, poorer performance is observed. This is most probably due to a drying out of the MEA on the cathodic side. A 15-h continuous-discharge test at 500 mV and at 120 °C for the same cell, without recycling the water or compensating for the

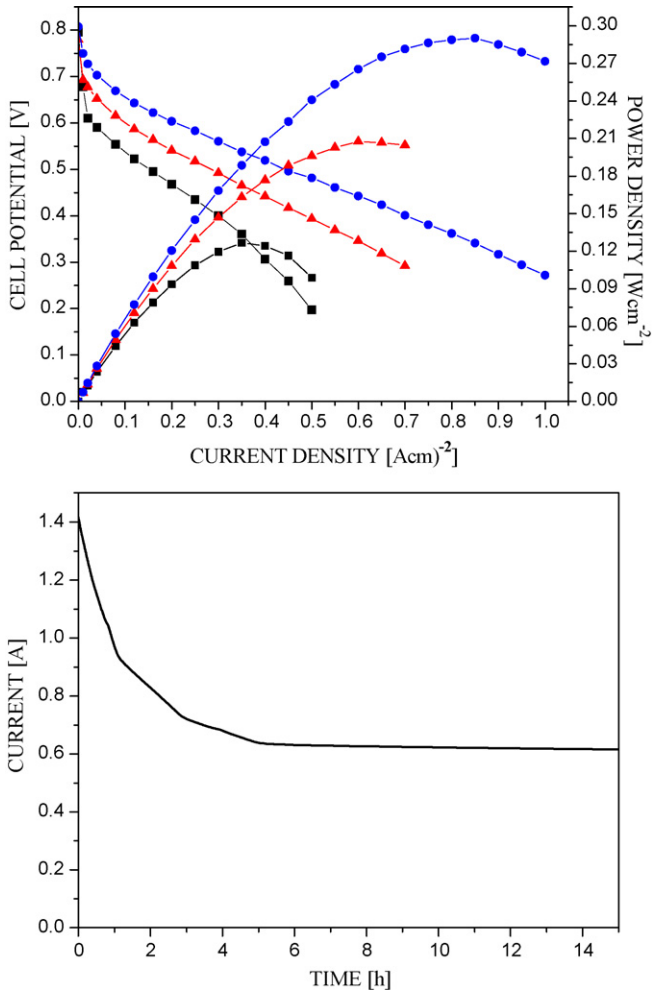

Fig. 12. (a) Cell polarization and power curves for 5-cm^2-area DMFC containing ∼100 μm SASA-based membrane (12%, w/w, ceramic powder), E-TEK® cathode and homemade anode (4 mg Pt cm^{-2}) in 1 M MeOH: (■) 80 °C: 127 mW cm^{-2} at 0.05 bar, 90 mL min^{-1} (air), 1.6 stoich (air) at 0.5 A cm^{-2}. (▲) 110 °C: 208 mW cm^{-2} at 1.2 bar, 245 mL min^{-1} (air), 6.3 stoich (air) at 0.7 A cm^{-2}. (●) 130 °C: 290 mW cm^{-2} at 3.0 bar, 177 mL min^{-1} (air), 5.5 stoich (air) at 1.0 A cm^{-2}. (b) 15-h continuous discharge test at 500 mV at 120 °C, without recycling water or compensating for the methanol concentration consumed.

methanol concentration consumed, shows a 57% decrease in performance, compared with initial data (Fig. 12b). The drop in current began at 1.42 A and became constant at 0.62 A. During the discharge test dry air was fed at 70 mL min^{-1}, 2.0 bar and at 5.5 stoich at 0.3 A cm^{-2}.

Although, the membrane conductivity is about one-half of that measured for Nafion®, the DMFC power achieved so far is close to the state-of-the-art level. The characteristics of the SASA-based CPEM measured in this work make it a promising candidate for fuel-cell applications. Although this work is only preliminary, it is considered that the new concept of a PEM with a functionalized ceramic powder containing SASA has given results that clearly indicate further research. Work is in progress on the optimization of SASA-based membranes and MEA preparation with a view to reducing cell resistance, and on the search for application in hydrogen fuel cells.

4. Summary

A novel PEM based on a single-step preparation of functionalized ceramic powder containing SASA and a polymer binder has been synthesized and characterized for the first time. The work includes the various stages of preparation of the membrane.

Several precursors have been examined, of which precursor (iii) in toluene is chosen, since its SASA powder shows the lowest EW (1281 g equiv.$^{-1}$).

The membrane has promising properties: PSD measurements reveal that a typical pore in the membrane has a diameter of 2–50 nm, high thermal stability (up to 250 °C), pressure–retention difference of at least 4 bar, and a high water-flow hydraulic permeation under low pressure.

Performance tests of a DMFC incorporating a SASA-based membrane show that the cell resistance for a ∼100-μm-thick membrane ranges between 0.29 and 0.19 Ω cm^2 at 80 and 130 °C, respectively, and that the maximum cell power density with a 1 M methanol solution is 127, 208 and 290 mW cm^{-2} at 80, 110 and 130 °C, respectively. The methanol crossover current density measured in a 1 M methanol solution is 0.093, 0.238 and 0.281 A cm^{-2} at 80, 110 and 130 °C, respectively. Further research is in progress on the optimization of SASA-based membranes with a view to reducing the cell resistance, as well as improving the MEA preparation, and applying it in hydrogen fuel cells.

Acknowledgements

The authors are grateful to Prof. Diana Golodnitsky of The Wolfson Applied Materials Research Center at Tel-Aviv University for assistance with comprehensive characterization of the synthesized materials, and to the Israel Plastics and Rubber Center (IPRC) for their kind provision of materials and equipment.

References

[1] M. Doyle, G. Rajendran, in: W. Vielstich, A. Lamm, H.A. Gasteiger (Eds.), Handbook of Fuel Cells, John Wiley & Sons Inc., New Jersey, 2003, pp. 351–395.
[2] K. Prater, J. Power Sources 29 (1990) 239–250.
[3] S. Srinivasan, J. Electrochem. Soc. 136 (1989) 41C–48C.
[4] P. Costamagna, S. Srinivasan, J. Power Sources 102 (2001) 242–252.
[5] Y. Woo, S.Y. Oh, Y.S. Kang, B. Jung, J. Membr. Sci. 220 (2003) 31–45.
[6] T.I. Valdez, S.R. Narayanan, in: S. Gottesfeld, T.F. Fuller (Eds.), Proceedings of the Second International Symposium on Proton Conducting Membrane Fuel Cells II, PV 98-27, The Electrochemical Society Proceedings Series, New Jersey, 1999, pp. 380–387.
[7] X. Ren, T.E. Springer, T.A. Zawodzinski, S. Gottesfeld, J. Electrochem. Soc. 147 (2000) 466–474.
[8] R. Jiang, D. Chu, J. Electrochem. Soc. 151 (2004) A69–A76.
[9] B. Smitha, S. Sridhar, A.A. Khan, J. Membr. Sci. 259 (2005) 10–26.
[10] S. Faure, N. Cornet, G. Gebel, R. Mercier, M. Pineri, B. Sillion, in: O. Savadogo, P.R. Roberge (Eds.), Proceedings of the Second International Symposium on New Materials for Fuel Cell and Modern Battery Systems II, École Polytechnique de Montréal, Canada, 1997, pp. 818–827.
[11] D.E. Curtin, R.D. Lousenberg, T.J. Henry, P.C. Tangeman, M.E. Tisack, J. Power Sources 131 (2004) 41–48.
[12] E. Peled, T. Duvdevani, A. Melman, Electrochem. Solid-State Lett. 1 (1998) 210–211.

[13] J. Kerres, W. Cui, M. Junginger, J. Membr. Sci. 139 (1998) 227–241.
[14] D.J. Jones,. Rozière, J. Membr. Sci. 185 (2001) 41–58.
[15] N. Cornet, O. Diat, G. Gebel, F. Jousse, D. Marsacq, R. Mercier, M. Pineri, J. New Mater. Electrochem. Syst. 3 (2000) 33–42.
[16] G. Hübner, E. Roduner, J. Mater. Chem. 9 (1999) 409–418.
[17] J.J. Sumner, S.E. Creager, J.J. Ma, D.D. DesMarteau, J. Electrochem. Soc. 145 (1998) 107–110.
[18] K.D. Kreuer, Solid State Ionics 97 (1997) 1–15.
[19] J. Kerres, A. Ullrich, F. Meier, T. Häring, Solid State Ionics 125 (1999) 243–249.
[20] E. Peled, T. Duvdevani, A. Aharon, A. Melman, Electrochem. Solid-State Lett. 3 (2000) 525–528.
[21] E. Peled, T. Duvdevani, A. Aharon, A. Melman, Electrochem. Solid-State Lett. 4 (2001) A38–A41.
[22] E. Peled, V. Livshits, T. Duvdevani, J. Power Sources 106 (2002) 245–248.
[23] A. Blum, T. Duvdevani, M. Philosoph, N. Rudoy, E. Peled, J. Power Sources 117 (2003) 22–25.
[24] E. Peled, A. Blum, A. Aharon, M. Philosoph, Y. Lavi, Electrochem. Solid-State Lett. 6 (2003) A268–A271.
[25] S. Reichman, T. Duvdevani, A. Aharon, M. Philosoph, D. Golodnitsky, E. Peled, J. Power Sources 153 (2006) 228–233.
[26] S. Reichman, A. Ulus, E. Peled, J. Electrochem. Soc. 154 (2007) B327–B333.
[27] T. Duvdevani, M. Philosoph, M. Rakhman, D. Golodnitsky, E. Peled, J. Power Sources 161 (2006) 1069–1075.
[28] K. Moller, T. Bein, Chem. Mater. 10 (1998) 2950–2963.
[29] J.H. Clark, D.J. Macquarrie, Chem. Commun. 8 (1998) 853–860.
[30] G.E. Fryxell, J. Liu, T.A. Hauser, Z. Nie, K.F. Ferris, S. Mattigod, M. Gong, R.T. Hallen, Chem. Mater. 11 (1999) 2148–2154.
[31] D. Brunel, Micropor. Mesopor. Mater. 27 (1999) 329–344.
[32] R.W. Murray, in: A.J. Bard (Ed.), Electroanalytical Chemistry, vol. 13, Marcel Dekker Inc., New York, 1984, p. 191.
[33] O. Lev, Z. Wu, S. Bharathi, V. Glezer, A. Modestov, J. Gun, L. Ravinovich, S. Sampath, Chem. Mater. 9 (1997) 2354–2375.
[34] J.T. Wang, S. Wasmus, R.F. Savinell, J. Electrochem. Soc. 143 (1996) 1233–1239.
[35] M. Alvaro, A. Corma, D. Das, V. Fornés, H. García, Chem. Commun. 8 (2004) 956–957.
[36] W.M. Van Rhijn, D.E. De Vos, B.F. Sels, W.D. Bossaert, P.A. Jacobs, Chem. Commun. 3 (1998) 317–318.
[37] D. Das, J.F. Lee, S. Cheng, Chem. Commun. 21 (2001) 2178–2179.
[38] T.A. Zawodzinski, T.E. Springer, J. Davey, R. Jestel, C. Lopez, J. Valerio, S. Gottesfeld, J. Electrochem. Soc. 140 (1993) 1981–1985.
[39] G. Michael, H. Ferch, Technical Bulletin Pigments, Basic Characteristics and Applications of AEROSIL®, vol. 11, Degussa AG, 1993.
[40] P.J. James, J.A. Elliott, T.J. McMaster, J.M. Newton, A.M.S. Elliott, S. Hanna, M.J. Miles, J. Mater. Sci. 35 (2000) 5111–5119.
[41] H.G. Haubold, T. Vad, H. Jungbluth, P. Hiller, Electrochim. Acta 46 (2001) 1559–1563.
[42] N. Furukawa, H. Fujihara, in: S. Patai, Z. Rappoport (Eds.), The Chemistry of Sulphonic Acids, Esters and their Derivatives, John Wiley & Sons, England, 1991, pp. 261–281.
[43] H. Ghassemi, J.E. McGrath, T.A. Zawodzinski, Polymer 47 (2006) 4132–4139.
[44] J.F. Moulder, W.F. Stickle, P.E. Sobol, K.D. Bomben, Handbook of X-Ray Photoelectron Spectroscopy, Perkin-Elmer Corporation, Physical Electronics Division, 1992.
[45] G. Beamson, D. Briggs, High Resolution XPS of Organic Polymers, John Wiley & Sons, England, 1992.
[46] P.C. Rieke, N.E. Vanderborgh, J. Membr. Sci. 32 (1987) 313–328.
[47] G. Alberti, M. Casciola, L. Massinelli, B. Bauer, J. Membr. Sci. 185 (2001) 73–81.
[48] M. Doyle, M.E. Lewittes, M.G. Roelofs, S.A. Perusich, J. Phys. Chem. B 105 (2001) 9387–9394.
[49] T.E. Springer, T.A. Zawodzinski, S. Gottesfeld, J. Electrochem. Soc. 138 (1991) 2334–2342.
[50] Y. Sone, P. Ekdunge, D. Simonsson, J. Electrochem. Soc. 143 (1996) 1254–1259.
[51] R.W. Kopitzke, C.A. Linkous, H.R. Anderson, G.L. Nelson, J. Electrochem. Soc. 147 (2000) 1677–1681.
[52] Y.W. Park, N. Inagaki, Polymer 44 (2003) 1569–1575.
[53] S.A. Cho, E.A. Cho, I.-H. Oh, H.-J. Kim, H.Y. Ha, S.-A. Hong, J.B. Ju, J. Power Sources 155 (2006) 286–290.
[54] P. Choi, R. Datta, J. Electrochem. Soc. 150 (2003) E601–E607.
[55] L. Yan, Y.S. Li, C.B. Xiang, Polymer 46 (2005) 7701–7706.